OPERATING CHARACTERISTICS FOR DETECTION OF PROCESS CHANGE PART 2: COMPUTATION OF PERFORMANCE MEASURES

Stephen M. Pollock
Department of Industrial and Operations Engineering
The University of Michigan
Ann Arbor, MI 48109-2117

and

Jeffrey M. Alden
GM NAO R&D Center
Warren, MI 48090

Technical Report 93-33

November 1993

1. Introduction

In this paper we explore the numerical computation of the performance measures associated with the monitoring policy described in Pollock and Alden (1992), hereafter referred to as P&A. In particular, we present a numerical approximation method to solve equations (A3), (A4), and (A5) in P&A. As shown in P&A, this is equivalent to finding steady state solutions for the state probabilities of the approximating Markov chain MCZ of Appendix B.

2. Computing Performance Measures given $\tilde{P}$.

We recall, from Appendix B of P&A, that the state space of MCZ is $\{0, 1, 2, \ldots 2m\}$. The "renewal" state is $\{0\}$, the false alarm state is $\{m\}$, the true alarm state is $\{2m\}$, the set $\{1, 2, \ldots, m-1\}$ represents states where the system is in condition G, and the set $\{m+1, m+2, \ldots 2m-1\}$ represents states where the system is in condition B.

We first assume that the $(2m+1) \times (2m+1)$ transition probability matrix $\tilde{P}$ is available, where

$$[\tilde{P}]_{ij} = \text{prob. } \{Z_{n+1} = j \mid Z_n = i\} \quad i,j = 0,1,2,\ldots 2m,$$

and Z_n is the MCZ state after observating X_n. Sections [3] and [6] provide the elements of $\tilde{P}$ for Bernoulli and Normal observations, respectively.

The steady state probability vector $\tilde{\pi}$, where

$$\tilde{\pi} \equiv (\pi_0 \ \pi_1 \ \ldots \ \pi_{2m}),$$

is then obtained from the Chapman-Kolmogorov equation

$$\tilde{\pi} = \tilde{\pi}\tilde{P} \tag{1}$$

2

along with the "normalizing" equation

$$\sum_{i=0}^{2m} \pi_i = 1. \tag{2}$$

$\tilde{P}$ can be expressed in terms of a $2m \times 2m$ matrix P, a $2m$-dimensional row vector p_0 and a $2m$-dimensional column vector p_1:

$$\tilde{P} = \begin{bmatrix} 0 & p_0 \\ p_1 & P \end{bmatrix} \tag{3}$$

and $\tilde{\pi}$ can be written in terms of π_0 and the $2m$-dimensional row vector $\pi \equiv (\pi_1 \ \pi_2 \ldots \pi_{2m})$, so that $\tilde{\pi} = (\pi_0 \ \pi)$. (Recall $\pi_0 \equiv$ steady-state probability the system occupies the renewal state. This in turn equals the checking rate, since the renewal state sojourn time is assumed to be 1.)

This allows equations (1) and (2) to be written

$$(\pi_0 \ \pi) = (\pi_0 \ \pi) \begin{pmatrix} 0 & p_0 \\ p_1 & P \end{pmatrix} \tag{4}$$

and

$$\pi_0 + \pi\mathbf{1} = 1 \tag{5}$$

where $\mathbf{1} \equiv (1 \ 1 \ 1 \ \ldots \ 1)'$ is the unit $2m$-dimensional column vector.

Equation (4) can then be written as the equation

$$\pi_0 = \pi p_1 \tag{6}$$

and the set of equations

$$\pi = \pi_0 p_0 + \pi P. \tag{7}$$

3

From the development in P&A and the definition of p_1, we know that p_1 has elements of 1 in the mth and $2m^{th}$ rows only, and is zero everywhere else. Thus equation (6) reduces to

$$\pi_0 = \pi_m + \pi_{2m} = \pi_G^* + \pi_B^*$$

where

$\pi_G^* = $ steady state probability system is in the "true alarm" state, and

$\pi_B^* = $ steady state probability system is in the "false alarm" state.

As shown in P&A, the structure of the transition matrix P allows it to be further decomposed as

$$P = \begin{pmatrix} (1-a)G & aB \\ 0 & B \end{pmatrix} \tag{8}$$

where: $a = $ probability of transition from condition G to condition B in a single time period; G is the $m \times m$ matrix, with elements G_{ij} describing Z_n-transitions while the system is in condition G, and B is the $m \times m$ matrix, with elements B_{ij}, describing Z_n-transitions while the system is in condition B. Note the mth row of both G and B contains all zeros, since the next state from an alarm state must be the renewal state.

We can represent the row vector p_0, which represents probabilities of transition from the renewal state to all other states, by

$$p_0 = [(1-a)g \quad ab] \tag{9}$$

where g and b are m-dimensional row vectors with components g_i and b_i. Similarly, the steady state vector π can be written

$$\pi = [\pi_g \quad \pi_b]. \tag{10}$$

With these representations, equations (7) become

$$[\pi_g \; \pi_b] = \pi_0[(1-a)g \; ab] + [\pi_g \; \pi_b] \begin{bmatrix} (1-a)\,G & aB \\ 0 & B \end{bmatrix} \tag{11}$$

or the two sets of linear equations:

$$\pi_g = (1-a)\pi_0 g + (1-a)\pi_g G \tag{12}$$

and

$$\pi_b = a\pi_0 b + a\pi_g B + \pi_b B. \tag{13}$$

The normalization condition of equation (5) can be re-stated as:

$$\pi_0 + \pi_g \mathbf{1} + \pi_b \mathbf{1} = 1. \tag{14}$$

The method of computation begins by letting $\hat{\pi}_g \equiv \pi_g/\pi_0$ and $\hat{\pi}_b = \pi_b/\pi_0$; then equations (12), (13) and (14) become

$$\hat{\pi}_g[\mathbf{I} - (1-a)G] = (1-a)g \tag{15}$$

$$\hat{\pi}_b[\mathbf{I} - \mathbf{B}] = ab + a\hat{\pi}_g B \tag{16}$$

$$\pi_0 = (1 + \hat{\pi}_g \mathbf{1} + \hat{\pi}_b \mathbf{1})^{-1}. \tag{17}$$

Equation (15) is readily solved for $\hat{\pi}_g$, since it is a set of m linear equations in m unknowns. Once $\hat{\pi}_g$ is obtained, equation (16) can be solved for $\hat{\pi}_b$ — another set of m linear equations. Finally, π_0 is obtained from equation (17), which gives

$$\pi_g = \hat{\pi}_g \pi_0 \tag{18}$$

$$\pi_b = \hat{\pi}_b \pi_0. \tag{19}$$

Some performance measures of interest are

5

π_0 = checking rate, obtained from (17)

π_G^* = false alarm rate: the mth element of π_g obtained from equation (18)

p_B = prob.{system is in condition B}

= $\pi_b 1$ found by summing the elements in π_b obtained from equation (19).

3. Elements of $\tilde{P}$ for Bernoulli monitoring

In the case of Bernoulli monitoring, we observe random variables $X_n = 0$ or 1, with distribution $p(x)$ when in condition G given by

$$p(x) = \begin{cases} 1 - \alpha & \text{if } x = 0 \\ \alpha & \text{if } x = 1 \end{cases}$$

and distribution $q(x)$ when in condition B given by

$$q(x) = \begin{cases} \beta & \text{if } x = 0 \\ 1 - \beta & \text{if } x = 1. \end{cases}$$

As shown in Section 9 of P&A, by defining

$$w_0 = \frac{\beta}{(1-a)(1-\alpha)}$$
$$w_1 = \frac{1-\beta}{(1-a)\alpha}$$

the evolution of the monitored Z_n process is governed by

$$Z_{n+1} = \begin{cases} w_0(Z_n + 1) & \text{if } X_{n+1} = 0 \\ w_1(Z_n + 1) & \text{if } X_{n+1} = 1. \end{cases} \tag{20}$$

Selecting the value of m, which determines the dimension of G, g, B and b, is related to the desired accuracy of the computation of performance measures. As noted in P&A, the number of possible states occupied by the Z_n process (MPZ) generated by equation (20)

6

is generally unbounded. Selecting a value of m is equivalent to determining the degree to which the discrete state approximation (MCZ) represents MPZ. For the moment, we assume m is given (determining a value for m is left to section 4).

The key issues in determining the elements of G, g, B and b are

a) identifying a set of z-values $S \equiv \{z_i : i = 0, 1, \ldots, m\}$, where $z_0 = 0$ and $z_m = z^*$;

b) associating each Z_n-value generated by equation (20) with an element in S.

We use an arbitrary but simple method for item b): assign Z_{n+1} to the element $z_k \in S$ that is closest in absolute value. This is expressed mathematically as

$$J_0(i) = \arg \min_{k=0,1,\ldots,m} \{| w_0(z_i + 1) - z_k |\}$$

$$J_1(i) = \arg \min_{k=0,1,\ldots,m} \{| w_1(z_i + 1) - z_k |\}$$

The elements of the matrices G and B needed for solving equation (15), (16), and (17) are

$$g_j = \begin{cases} (1 - \alpha) & \text{if } j = J_0(0) \\ \alpha & \text{if } j = J_1(0) \\ 0 & \text{other } j \end{cases}$$

$$G_{ij} = \begin{cases} (1 - \alpha) & \text{if } j = J_0(i), \quad i = 1, 2, \ldots m - 1 \\ \alpha & \text{if } j = J_1(i), \quad i = 1, 2, \ldots m - 1 \\ 0 & \text{other } j, \quad i = 1, 2, \ldots m - 1 \\ 0 & \text{all } j, \quad i = m \end{cases}$$

7

$$b_j = \begin{cases} \beta & \text{if } j = J_0(0) \\ 1 - \beta & \text{if } j = J_1(0) \\ 0 & \text{other } j \end{cases}$$

$$B_{ij} = \begin{cases} \beta & \text{if } j = J_0(i), & i = 1, 2, \ldots m - 1 \\ 1 - \beta & \text{if } j = J_1(i), & i = 1, 2, \ldots m - 1 \\ 0 & \text{other } j, & i = 1, 2, \ldots m - 1 \\ 0 & \text{all } j, & i = m. \end{cases}$$

4. Algorithm for defining $\{z_i\}$

Defining the subset $\{z_1, z_2, \ldots, z_{m-1}\}$ of S is somewhat arbitrary. A simple algorithm that seems to provide numerically stable performance measures is to generate all possible z-values over a "horizon" of h observations of X. The advantages of this approach are:

- only feasible z-values are generated,

- it accurately represents the Z_n process over the horizon, and

- the value of m, and consequently the accuracy of the approximation, can be increased by increasing h (see Section [5]).

The algorithm follows:

Algorithm for generating m and $S \equiv \{z_i\}_{i=0}^m$

1. Set $S_0 = \{0, z^*\}$.

8

2. Select a horizon $h \geq 1$.

3. Set $n = 1$.

4. Generate $s_0 = \{w_0(z_i + 1) : z_i \in S_{n-1}$ and $w_0(z_i + 1) < z^*\}$.

5. Generate $s_1 = \{w_1(z_i + 1) : z_i \in S_{n-1}$ and $w_1(z_i + 1) < z^*\}$.

6. Set $S_n = \{z : z \in s_0 \cup s_1$ and $z \notin \cup_{i=0}^{n-1} S_i\}$.

7. Increment n by 1.

8. If $n < h$ then go to step 4.

9. Set $S = \cup_{i=0}^{n} S_i$ and set $m = |S| - 1$.

At termination, the set S will be a set of $m + 1$ distinct z-values which, when sorted by increasing value, can be labeled $z_0, z_1, z_2, \ldots, z_m$. Thus, given values of α, β, a, and z^*, as well as the horizon h, the algorithm provides a value of m and set S. A larger h generally produces a larger m. It is easy to show that $m \leq 2^h$. Our computational experience has often shown that m increases close to exponentially in h.

5. Elements of $\dot{P}$ for Normal monitoring.

In the case of Normal monitoring, the X_n are independent normally distributed random variables with distribution parameters depending only on system condition. Without loss of generality, we assume the distribution of X_n is $p(x)$ with mean $= 0$ and standard deviation $= 1$ while in condition G, and is $q(x)$ with mean $= \mu$ and standard deviation $= 1$ while in condition B:

$$p(x) = \frac{1}{\sqrt{2\pi}} e^{-x^2/2}$$

9

$$q(x) = \frac{1}{\sqrt{2\pi}} e^{-(x-\mu)^2/2}.$$

The likelihood ratio is

$$L(x) = q(x)/p(x) = e^{\mu x - \mu^2/2}$$

and equation (16) of P&A becomes

$$Z_{n+1} = \gamma e^{\mu X_n}[1 + Z_n],$$

where

$$\gamma = \frac{e^{-\mu^2/2}}{1 - a}.$$

Again, we assume the set of Z-values $\{z_0 \equiv 0, z_1, z_2, \ldots, z_{m-1}, z_m \equiv z^*\}$ is given. Then, using the governing equation (20) given $Z_n = y$, we compute the cumulative distribution of Z_{n+1}, from which the associated pdf can be obtained:

$$\begin{aligned}
\text{prob.}\{Z_{n+1} \le z\} &= \text{prob.}\{\gamma e^{\mu X_n}(1 + y) \le z\} \\
&= \text{prob.}\{X_n \le \frac{1}{\mu} \ln \frac{z}{\gamma(1+y)}\}.
\end{aligned}$$

When the system is in condition G, X_n has pdf $p(x)$. Thus the elements of G are given by

$$\begin{aligned}
G_{ij} &= \text{prob.}\{Z_{n+1} = z_j \mid Z_n = z_i\} \\
&= \text{prob.}\{Z_{n+1} \le z_j \mid Z_n = z_i\} - \text{prob.}\{Z_{n+1} \le z_{j-1} \mid Z_n = z_i\} \\
&= \Phi\left(\frac{1}{\mu} \ln \frac{z_j}{\gamma(1 + z_i)}\right) - \Phi\left(\frac{1}{\mu} \ln \frac{z_{j-1}}{\gamma(1 + z_i)}\right) \qquad i, j = 1, 2, \ldots, m - 1.
\end{aligned}$$

where $\Phi(\cdot)$ is the standard normal cumulative distribution. By definition, we also have

$$G_{mj} = 0 \qquad j = 1, 2, \ldots, m.$$

Since state $z_m = z^*$ represents an alarm state,

$$[G]_{im} = \text{prob.}\{Z_{n+1} \ge z^* \mid Z_n = z_i\} = 1 - \Phi\left(\frac{1}{\mu} \ln \frac{z^*}{\gamma(1 + z_i)}\right) \qquad i = 1, 2, \ldots, m - 1.$$

10

Elements of g correspond to row "zero" of G, so that

$$
\begin{aligned}
g_j &= \text{prob.}\{Z_{n+1} = z_j \mid Z_n = 0\} \\
&= \Phi\left(\frac{1}{\mu}\ln\frac{z_j}{\gamma}\right) - \Phi\left(\frac{1}{\mu}\ln\frac{z_{j-1}}{\gamma}\right) \qquad j = 1,2,\ldots,m-1 \\
g_m &= 1 - \Phi\left(\frac{1}{\mu}\ln\frac{z^*}{\gamma}\right)
\end{aligned}
$$

By a similar argument, while the system is in condition B, X_n has pdf $q(x)$, and so

$$
\begin{aligned}
B_{ij} &= \Phi\left(\frac{1}{\mu}\ln\frac{z_j}{\gamma(1+z_i)} - \mu\right) - \Phi\left(\frac{1}{\mu}\ln\frac{z_{j-1}}{\gamma(1+z_i)} - \mu\right) & i,j &= 1,2,\ldots,m-1 \\
B_{mj} &= 0 & j &= 1,2,\ldots,m \\
B_{im} &= 1 - \Phi\left(\frac{1}{\mu}\ln\frac{z^*}{\gamma(1+z_i)} - \mu\right) & i &= 1,2,\ldots,m-1 \\
b_j &= \Phi\left(\frac{1}{\mu}\ln\frac{z_j}{\gamma} - \mu\right) - \Phi\left(\frac{1}{\mu}\ln\frac{z_{j-1}}{\gamma} - \mu\right) & j &= 1,2,\ldots,m-1 \\
b_m &= 1 - \Phi\left(\frac{1}{\mu}\ln\frac{z^*}{\gamma} - \mu\right).
\end{aligned}
$$

6. Computation for Normal monitoring

Exercising equations (15) through (17) for the Normal monitoring case requires a set $S \equiv \{z_i\}_{i=0}^m$ such that the resulting linear equations have numerically stable solutions as m becomes large. Because of the peculiar nature of the matrices G and B, defined in the preceding section, the task of generating an appropriate set S is difficult. Fortunately, however, X_n is a *continuous* random variable, which allows a re-stating of equations (15) through (17). This re-formulation allows their solution by means of existing techniques from numerical analysis. In particular, we define the elements of S to be

$$
z_i = i\Delta = \frac{iz^*}{m} \qquad i = 0,1,2,\ldots,m
$$

so that Δ is the interval between equally spaced points from $Z_n = 0$ and $Z_n = z^*$. This allows the definition of continuous analogues of the steady-state probability vectors $\hat{\pi}_g$ and $\hat{\pi}_b$; that is, we define $\hat{f}_g(z)$ and $\hat{f}_b(z)$ so that, in the limit as $\Delta \to 0$,

$$\pi_0 \hat{f}_g(z)\Delta \;=\; \text{(steady state) prob.}\{z < Z \le z+\Delta \cap \text{system is in condition } G\}$$

$$\pi_0 \hat{f}_b(z)\Delta \;=\; \text{(steady state) prob.}\{z < Z \le z+\Delta \cap \text{system is in condition } B\}$$

and so $\hat{f}_g(z_i)\Delta = [\hat{\pi}_g]_i$ and $\hat{f}_b(z_i)\Delta = [\hat{\pi}_b]_i$. Equation (15) can then be written

$$[\hat{\pi}_g]_j \;=\; (1-a)\sum_{i=1}^{m}[\hat{\pi}_g]_i G_{ij} + (1-a)g_j \quad j = 1,2,\ldots,m-1 \tag{21}$$

$$[\hat{\pi}_g]_m \;=\; (1-a)\sum_{i=1}^{m}[\hat{\pi}_g]_i G_{im} + (1-a)g_m. \tag{22}$$

Using the definition of $\hat{f}_g(.)$, the first set of these becomes:

$$\hat{f}_g(z_j)\Delta = (1-a)\sum_{i=1}^{m}\hat{f}_g(z_i)\Delta G_{ij} + (1-a)g_j \qquad j = 1,2,\ldots,m-1 \tag{23}$$

From the definitions of G_{ij} and g_j given in Section 5, it can be readily shown for small Δ and $i,j = 1,2,\ldots,m-1$ that

$$
\begin{aligned}
G_{ij} &\cong p\left(\frac{\Delta}{\mu}\ln\frac{z_j}{\gamma(1+z_i)}\right)\frac{d}{dz_j}\left[\frac{1}{\mu}\ln\frac{z_j}{\gamma(1+z_i)}\right] \\
&= \frac{\Delta}{\mu z_j}p\left(\frac{1}{\mu}\ln\frac{z_j}{\gamma(1+z_i)}\right)
\end{aligned}
$$

and

$$g_j \cong \frac{\Delta}{\mu z_j}p\left(\frac{1}{\mu}\ln\frac{z_j}{\gamma}\right).$$

Dividing equation (23) by Δ and taking the limit as $\Delta \to 0$ gives

$$\hat{f}_g(z) = (1-a)\int_0^{z^*}\hat{f}_g(x)\frac{1}{\mu z}p\left(\frac{1}{\mu}\ln\frac{z}{\gamma(1+x)}\right)dx + (1-a)\frac{1}{\mu z}p\left(\frac{1}{\mu}\ln\frac{z}{\gamma}\right) \quad 0 < z < z^* \tag{24}$$

By a similar argument,

$$\hat{f}_b(z) = \int_0^{z^*}[\hat{f}_b(x) + a\hat{f}_g(x)]\frac{1}{\mu z}q\left(\frac{1}{\mu}\ln\frac{z}{\gamma(1+x)}\right)dx + a\frac{1}{\mu z}q\left(\frac{1}{\mu}\ln\frac{z}{\gamma}\right) \quad 0 < z < z^* \tag{25}$$

Equations (23) and (24) are the continuous equivalents of equations (15) and (16). The solution method is essentially the same: we first solve equation (24) for $\hat{f}_g(z)$, and then

12

solve equation (25) for $\hat{f}_b(z)$. Substituting $G_{im} = 1 - \sum_{j=1}^{m-1} G_{ij}$ and $g_m = 1 - \sum_{j=1}^{m-1} g_j$ into equation (22) and then using the continuous approximations for G_{ij} and g_j, we can derive the alarm probabilities:

$$[\hat{\pi}_g]_m = (1-a) \int_0^{z^*} \hat{f}_g(x) \int_{z^*}^\infty \frac{1}{\mu z} p \left(\frac{1}{\mu} \ln \frac{z}{\gamma(1+x)} \right) dz\, dx + (1-a) \int_{z^*}^\infty \frac{1}{\mu z} p \left(\frac{1}{\mu} \ln \frac{z}{\gamma} \right) dz$$
(26)

$$[\hat{\pi}_b]_m = \int_0^{z^*} [\hat{f}_b(x) + a\hat{f}_g(x)] \int_{z^*}^\infty \frac{1}{\mu z} q \left(\frac{1}{\mu} \ln \frac{z}{\gamma(1+x)} \right) dz\, dx + a \int_{z^*}^\infty \frac{1}{\mu z} q \left(\frac{1}{\mu} \ln \frac{z}{\gamma} \right) dz.$$
(27)

Finally, the normalizing equation equivalent to equation (17) is

$$\pi_0^{-1} = 1 + \int_0^{z^*} \hat{f}_g(x) dx + \int_0^{z^*} \hat{f}_b(x) dx + [\hat{\pi}_g]_m + [\hat{\pi}_b]_m.$$
(28)

Equations (24) and (25) are Fredholm equations of the second kind, which, as pointed out in P&A, have been examined extensively in the literature. The key to their solution is the nature of their kernals, that is the behavior of

$$k_g(x,z) = \frac{1}{\mu z} p \left(\frac{1}{\mu} \ln \frac{z}{\gamma(1+x)} \right)$$

$$= \frac{1}{\mu z \sqrt{2\pi}} e^{-\frac{1}{2\mu^2} \ln^2 \frac{z}{\gamma(1+x)}}$$

and

$$k_b(x,z) = \frac{1}{\mu z \sqrt{2\pi}} e^{-\frac{1}{2} \left(\frac{1}{\mu} \ln \frac{z}{\gamma(1+x)} - \mu \right)^2}$$

In order to obtain a numerical solution to equation (24), a FORTRAN code was written using a NAG library subroutine (NAG, 1983) that solves this linear non-singular Fredholm integral equation of the second kind using the method of El-Gendi(1969). The function $\hat{f}_g(.)$, appearing on both sides of equation (24), is approximated by truncating a Chebychev

series to form an nth order polynomial. The subroutine solves for the resulting polynomial coefficients $c_i^g, i = 1, 2, \ldots, n$ such that

$$\hat{f}_g(z) \approx \sum_{i=1}^{n} c_i^g \cos\left((i-1)\cos^{-1}\left(\frac{2z}{z^*} - 1\right)\right) \tag{29}$$

with the property

$$\int_{z=0}^{z^*} \hat{f}_g(z)\, dz \approx \sum_{i=1; i \text{ odd}}^{n} \frac{c_i^g z^*}{1 - (i-1)^2}. \tag{30}$$

This analysis also provides $\hat{f}_g(x_i)$ evaluated over the set of Chebyshev points x_i where

$$x_i = \frac{z^*}{2}\left(1 + \cos\left(\frac{\pi(i-1)}{n-1}\right)\right) \qquad i = 1, 2, \ldots, n. \tag{31}$$

Equation (25) is then solved, using the same NAG subroutine, by approximating $\hat{f}_b(.)$ with a different Chebychev series and using $\hat{f}_g(.)$ obtained above. This produces the coefficients $c_i^b, i = 1, 2, \ldots, n$, such that

$$\hat{f}_b(z) \approx \sum_{i=1}^{n} c_i^b \cos\left((i-1)\cos^{-1}\left(\frac{2z}{z^*} - 1\right)\right), \tag{32}$$

with the property

$$\int_{z=0}^{z^*} \hat{f}_b(z)\, dz \approx \sum_{i=1; i \text{ odd}}^{n} \frac{c_i^b z^*}{1 - (i-1)^2}. \tag{33}$$

The performance measures $[\hat{\pi}_g]_m$ and $[\hat{\pi}_b]_m$ are obtained by trapezodial approximation of the integrals in equations (26) and (27) using the values of $\hat{f}_g(x_i)$ and $\hat{f}_b(x_i)$ obtained from equations (29) and (32) at the Chebyshev points x_i, $i = 1, 2, \ldots, n$. Finally, π_0 is obtained by substituting equations (30), (33), and the values of $[\hat{\pi}_g]_m$ and $[\hat{\pi}_b]_m$ into equation (28).

7. Numerical Results for Bernoulli Monitoring

In this section we present numerical results for Bernoulli monitoring. The first computation is generating m and the set S using the algorithm of section 4. Figures 7.1a, 7.1b, and

14

7.1c show how $m = |S|$ increases with increasing horizon h, for various values of α, β, a, and p^*. Comparison of these figures show how larger p^*, smaller a, and larger α and β increase the number of states generated for a given h.

7.1 Generating $S = \{z_i\}$

Figures 7.2a, 72.b, and 7.2c show the resulting z_i values and associated steady-state probabilities when $\alpha = \beta = 0.2$, $a = 0.01$, $p^* = 0.2$. Note the "jumpy" nature of the steady-state probabilities and the "gaps" in the z-axis. This behavior suggests that

a) any solution approach which uses a continuous approximation to the state space would be unwieldy, and

b) a using simple "grid" over the z axis to represent the possible z values would be inefficient due to computations associated with highly unlikely or even impossible z values.

Figure 7.2b suggests a possible fractal character of the z_i values by showing them in the region near zero ($0 \leq z_i \leq 5$) which produces a plot similar to Figure 7.2a.

Figure 7.2c shows how increasing the horizon from 8 to 12 (which increases the number of generated states) tends to fill in more values on the z axis but, has little effect on the predominant state probabilities.

The accuracy of the computations generally increases with h, as does the computational effort. Figure 7.3 illustrates how the increased accuracy (represented in the figure by the computed value of π_0) is unbiased and levels off near $h = 7$. Over a wide range of parameter settings, the maximum observed absolute percent error is less than 5 percent for $h \geq 7$. For this reason, we use $h = 7$ for the remaining computational results.

7.2 Operating Characteristics

In production management, a trade-off is often made between time spent producing

scrap and time spent "down" (i.e., not producing anything). In our analysis we know that increasing p^* reduces the down time due to false alarms yet this increases the time spent producing scrap. Such trade-offs can be captured by means of an operating characteristic (OC) curve (see P&A) which is created by plotting two competing performance measures as a function of a decision variable (such as p^*). Figures 7.4a, 7.4b, and 7.4c each show three OC curves (for $a \in \{0.1, 0.05, 0.01\}$) that plot $p_B = \Pr\{$system is in condition B$\} = \Pr\{$producing scrap$\}$ versus $\pi_0 = $ checking rate $= \Pr\{$down for checking$\}$ while varying p^* from 0.01 to 0.5. Figure 7.4a shows that, for a fairly non-informative sensor ($\alpha = \beta = 0.3$), varying p^* allows a wide range of operating points, with a resulting wide range of possible p_B and π_0 values. With a more sensitive sensor (Figure 7.4c with $\alpha = \beta = 0.1$), only a few operating points are possible for p^* between 0.01 and 0.5. Indeed, for $a = 0.1$ there is only one feasible operating point in this range of p^*: $p_B = 0.00747$ and $\pi_0 = 0.146$.

Figure 7.5 shows an OC for an "asymmetric" sensor having $\alpha = 0.3$ and $\beta = 0.2$. Note that improving only one error probability of the sensor, i.e., $\beta = \Pr\{x = 0|G\}$ from $\beta = 0.3$ (as in Figure 7.4a), improves both measures plotted in the OC. This is because a decrease in β reduces the time spent producing scrap by reducing the detection time. This also reduces the probability the system is down: a lower β gives greater confidence that $x = 0$ implies a good system; this reduces the upward drift in the Z_n process for a given set of observations containing zeros; finally, this delays the time until a false alarm occurs for a fixed alarm threshold.

Figure 7.6 compares different sensors for a system with $a = 0.01$. This OC allows an immediate assessment of the advantage of a more sensitive sensor. For example, if an operating policy with $\Pr\{B\} = 0.04$ is required, decreasing the error probabilities of the sensor from $\alpha = \beta = 0.3$ to $\alpha = \beta = 0.2$ decreases π_0 from about 0.11 to about 0.05.

Figure 7.7 shows an alternative form of an OC. The two attributes are p_B and $\Pr\{$Producing good product$\} = \pi_0 + p_G$. The latter measure is important since time spent checking causes

a decrease in production capacity even though there is less scrap produced. A fascinating result of this OC is the existance of operating points (above the dotted line) that are *never* optimal regardless of the (positive) cost per scrapped unit and (positive) revenue per good unit produced. For example when $a = 0.01$, there exits for each probability threshold p^* above 0.26 a p^* below 0.26 producing the same throughput of good product *and* a lower scrap rate.

8. Numerical Results for Normal Monitoring

Figure 8.1 shows the probability density function $\pi_0 \hat{f}_g(z)$ for Normal monitoring. Compared to Bernoulli monitoring (Figure 7.2) this distribution is smooth and well behaved except near zero where, it can be shown that $\lim_{z \to 0} \hat{f}_g(z) = 0$.

Figure 8.2 shows the Operating Characteristic Curves for $p_B = \Pr\{\text{Producing scrap}\}$ versus $\pi_0 = \Pr\{\text{Producing good product}\}$ for two values of a (0.05 and 0.1) while fixing $\mu = 1.5$. As in Figure 7.4a, there is an improvement in the OC with smaller a. Since a is the expected number of inter-monitoring intervals until system failure, a can be reduced by either increasing the actual life of a machine or by decreasing the inter-monitoring interval.

Figure 8.3 shows OC sensitivity to changing μ, the shift in the expected observation value when the system fails. As μ increases the power of the sensor to discriminate between conditions G and B increases and this improves the OC curve. This has obvious implications in evaluating sensors with different μ values.

Figure 8.4 shows the alternative OC curves for $\Pr\{\text{Producing scrap}\}$ versus $\Pr\{\text{Producing good product}\}$ for $a = 0.05$ and $\mu \in \{0.5, 1.0, 1.5\}$. As in Figure 7.7, if this OC represents a significant trade-off, then there is a wide range of probability thresholds that can be ignored when selecting an operating point. For example, when $\mu = .5$ and $a = 0.05$ all p^* above 0.15 can be ignored.

References

Pollock, S. M and Alden J. M., 1992, "Operating Characteristics for Detection of Process Change Part 1: Theoretical Development", Technical Report 92-34, IOE Dept., The University of Michigan.

NAG Fortran Library Routine, 1983, D05ABE, February 1983.

El-Gendi, S. E., 1969, "Chebyshev Solution of Differential, Integral and Integro-Differential Equations," *Computer Journal* 12, pp 282-287, 1969.

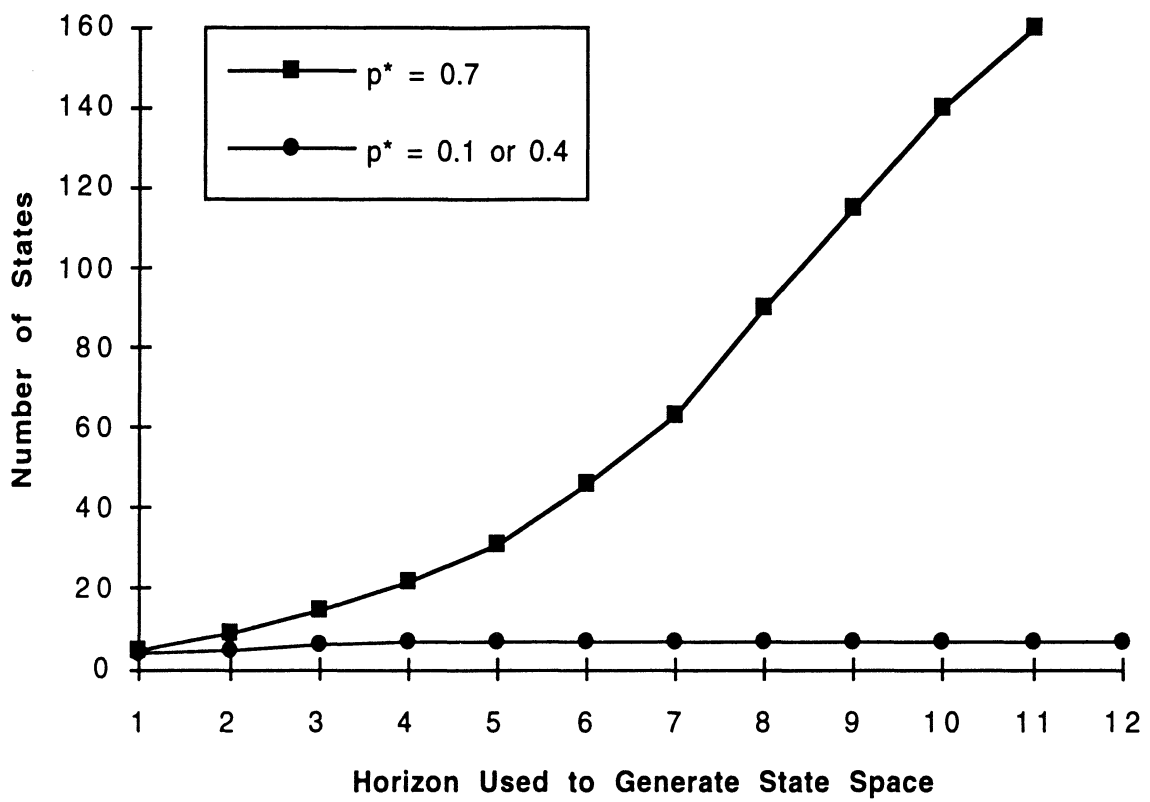**Bernoulli Monitoring: State Space Size**
a=0.1,   alpha=beta=0.15

Figure 7.1a: The number of states generated increases as the horizon used to generate the z-state space increases.

Bernoulli Monitoring: State Space Size
a=0.01,   alpha=beta=0.15
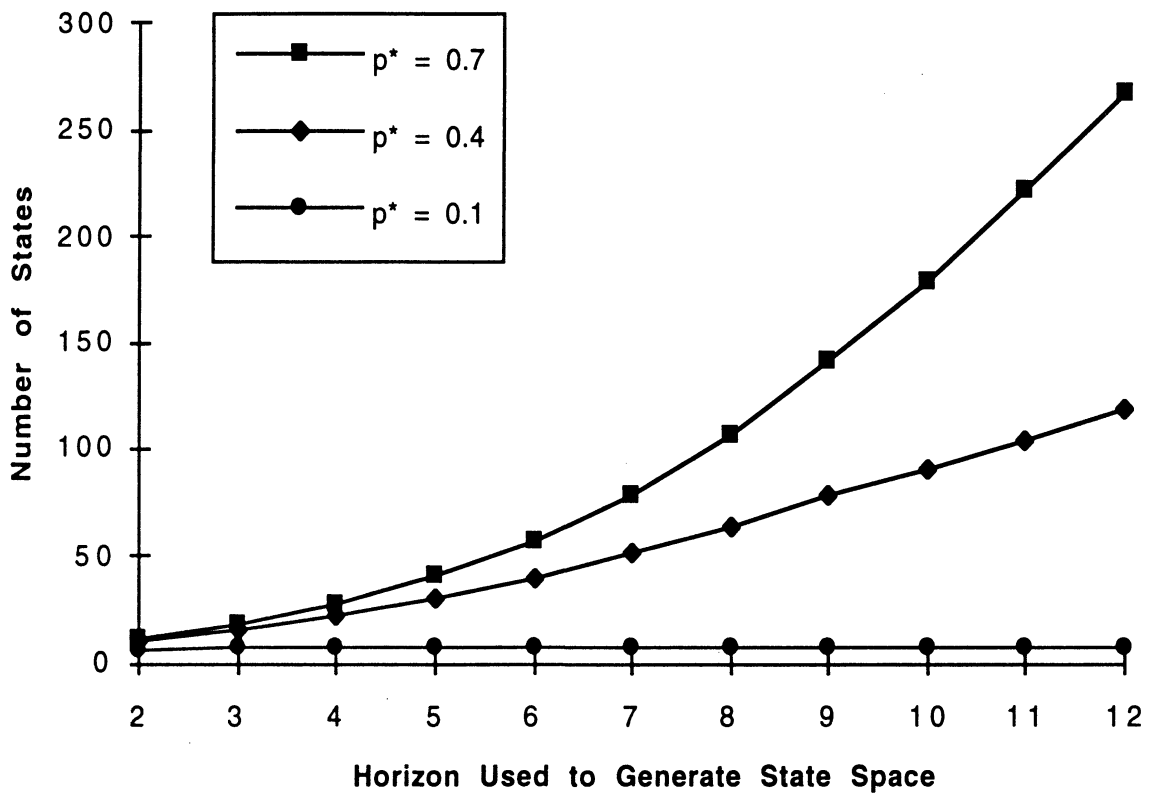
Figure 7.1b: Increasing mean time between failures by decreasing a from 0.1 (as in Figure 7.1a) to 0.01 (above) increases the number of generated states.

Bernoulli Monitoring: State Space Size

a=0.1,   alpha=beta=0.35
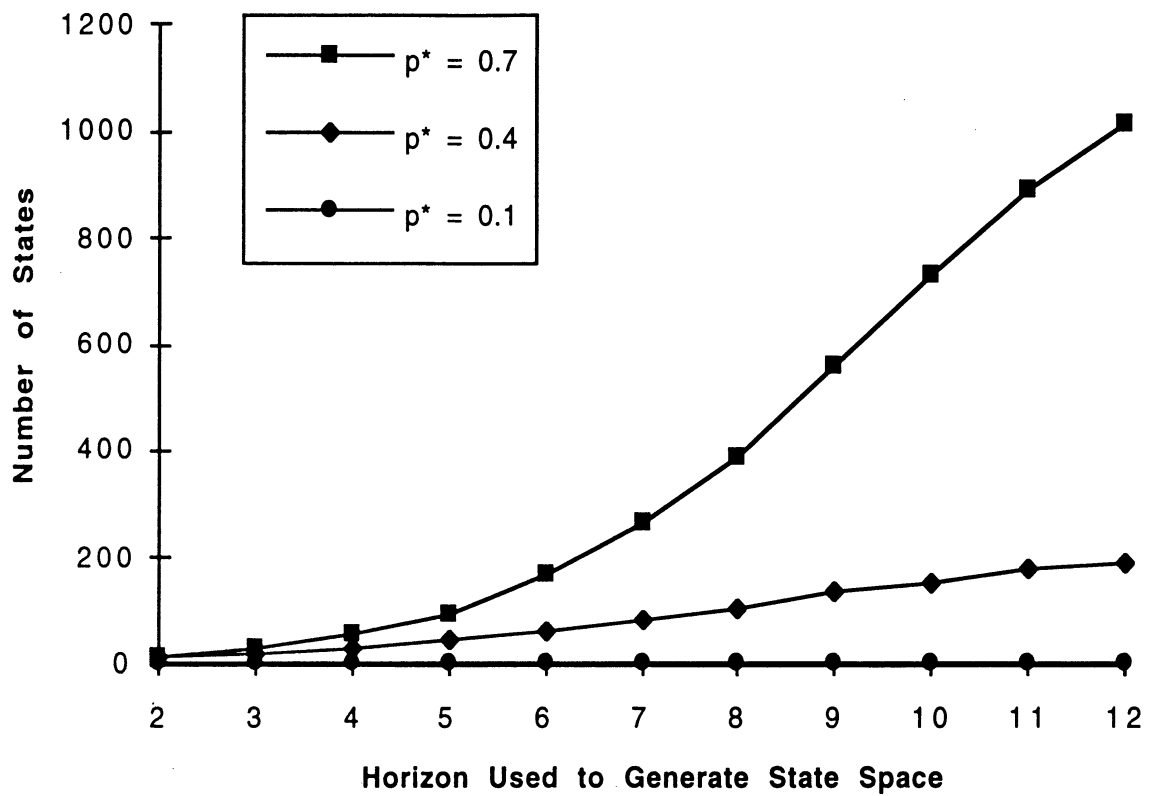
Figure 7.1c: Decreasing observation information content by increasing α and β from 0.15 (as in Figure 7.1a) to 0.35 (above) increases the number of generated states.

21

Bernoulli Monitoring: Probability Distribution over z
a=0.01,   alpha=beta=0.2,   p*=0.2,   h=8
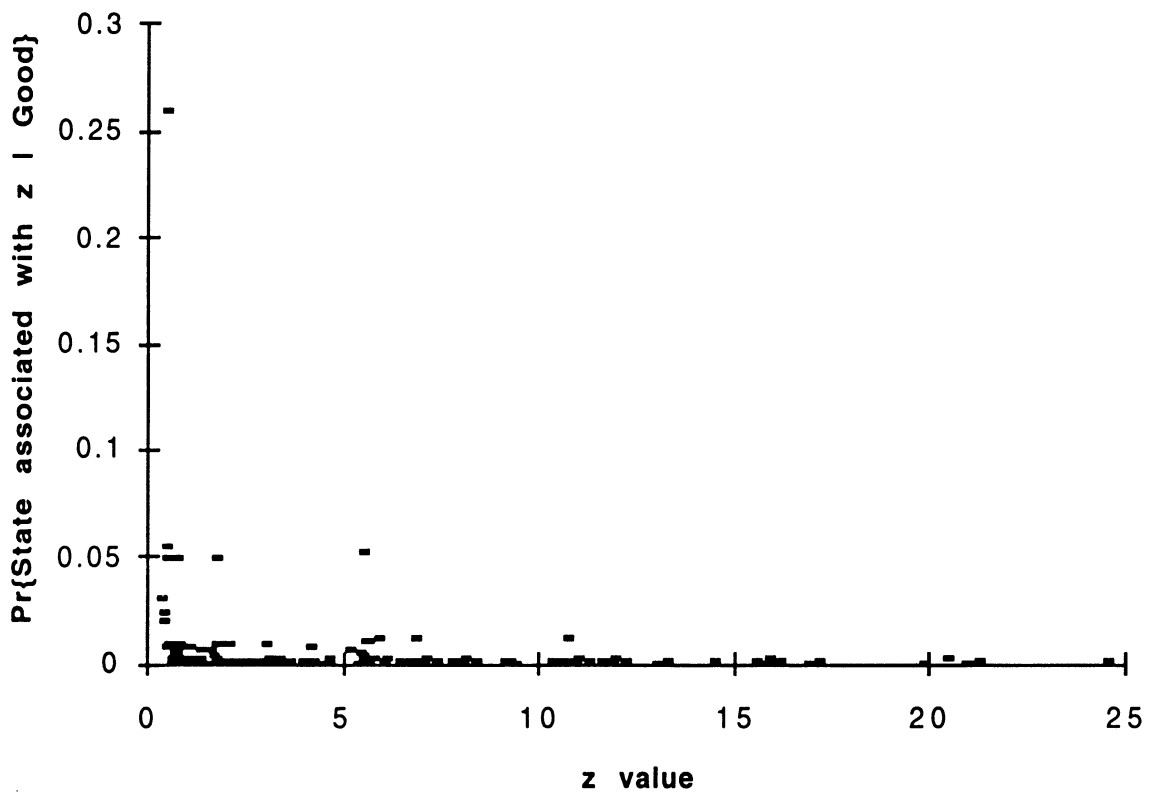
Figure 7.2a: The probability mass function $[\pi_g]_i$ associated with each z value generated by the solution proceedure when $\alpha = \beta = 0.2$, $a = 0.01$, $p^* = 0.2$, and a horizon of $h = 8$ is used to generate the state space.

Bernoulli Monitoring: Probability Distribution over z
a=0.01, alpha=beta=0.2, p*=0.2, h=8
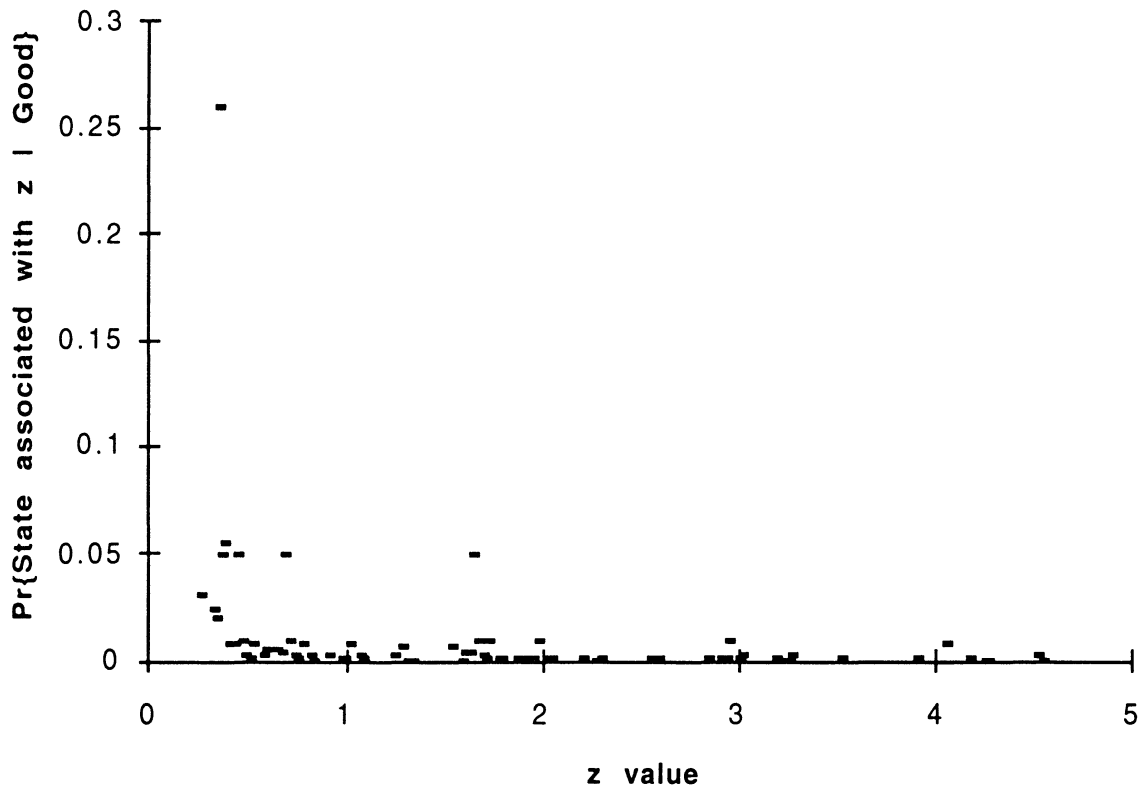
Figure 7.2b: $[\pi_g]_i$ of Figure 7.2a in the interval $0 \le z \le 6$ shows more detail. Note the "self similarity" of points in the interval $[1.5,2]$ to those in the interval $[5,7]$ of Figure 7.2a.

Bernoulli Monitoring: Probability Distribution over z
a=0.01,   alpha=beta=0.2,   p*=0.2,   h=12
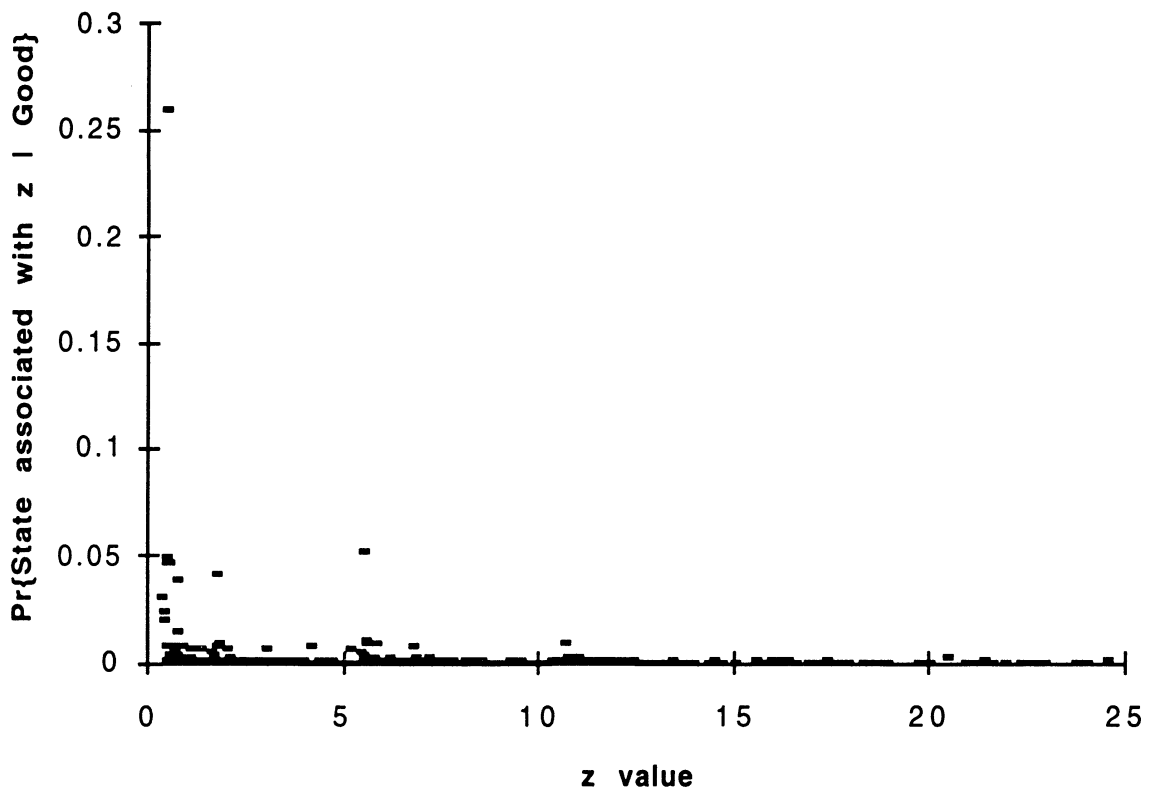
Figure 7.2c: Increasing the horizon h from 8 (as in Figure 7.2a) to 12 (above) introduces new z values, but has a minor effect on the probabilities associated with the old z values.

Bernoulli Monitoring: Convergence
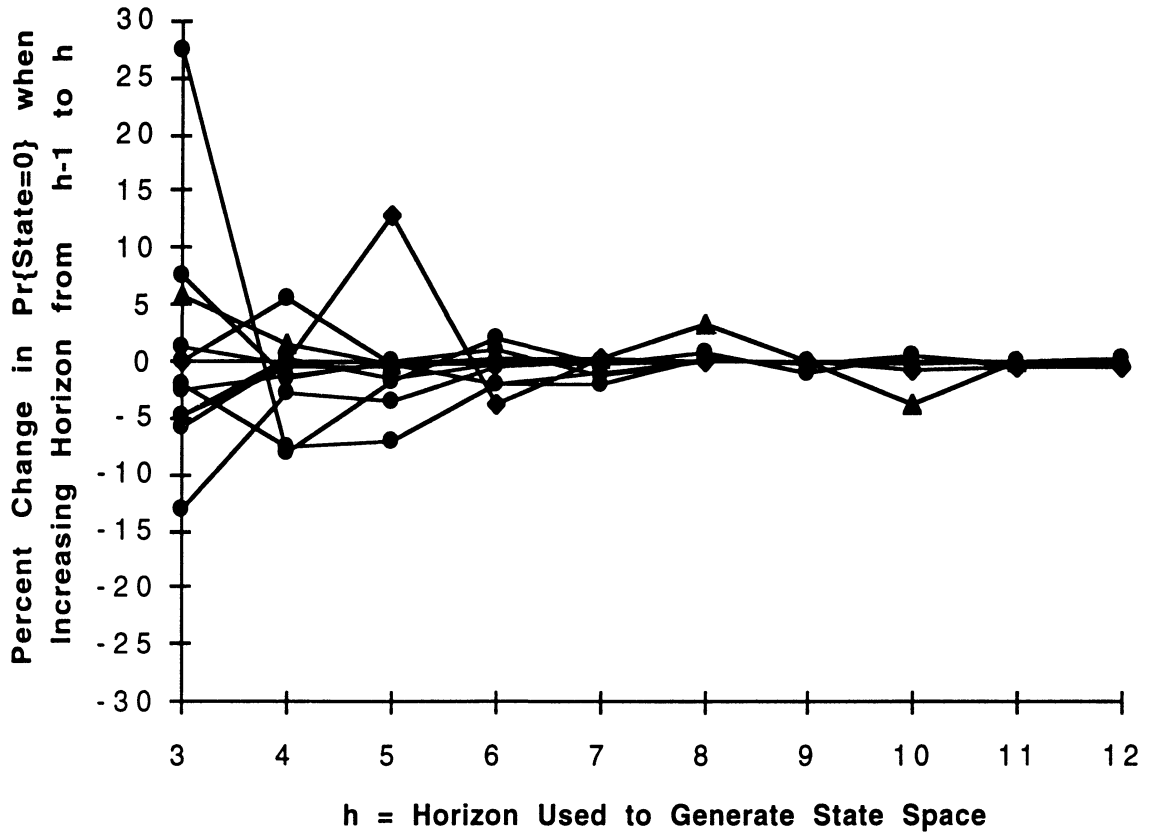
Figure 7.3: Percent change in π_0 as the horizon used to generate the z-state space increases from $h - 1$ to h. The figure displays 18 curves corresponding to all possible parameter settings such that $\alpha = \beta \in \{0.15, 0.25, 0.35\}$, $a \in \{0.01, 0.1\}$, and $p^* \in \{0.1, 0.4, 0.7\}$. Six of the parameter settings had zero percent change for all h shown. The two worst cases are plotted using diamonds ($\alpha = \beta = 0.35, a = 0.01, p^* = 0.4$) and triangles ($\alpha = \beta = 0.35, a = 0.01, p^* = 0.1$).

25
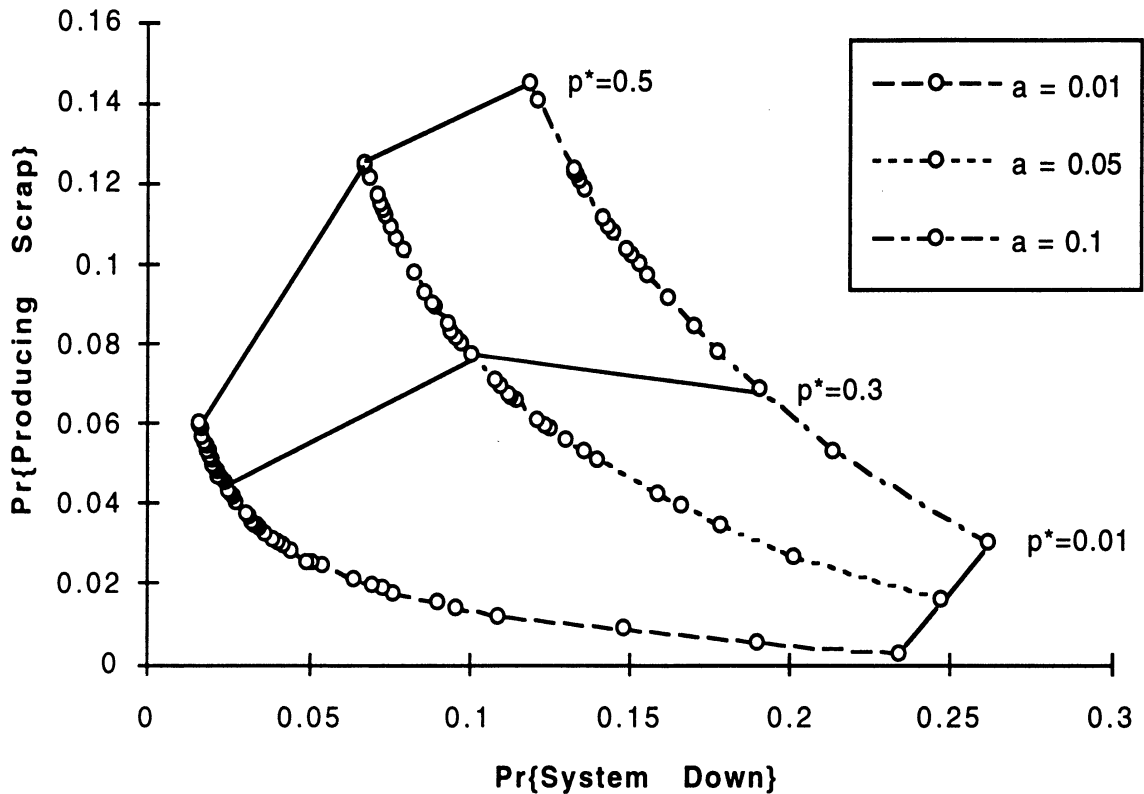
Figure 7.4a: Operating Characteristic Curves under Bernoulli monitoring for Pr{Producing Scrap} versus Pr{System Down} generated by varying p^* from 0.01 to 0.5 in steps of 0.01. There are three curves, one for each $a \in \{0.01, 0.05, 0.1\}$ with $\alpha = \beta = 0.3$ in each case. Any apparent non-convexity of these curves is due to round off errors in π_G^* and π_B^* which are used to calculate Pr{producing scrap} and Pr{system down}. Points associated with the same value of p^* are connected by solid lines for $p^* = 0.01$, 0.3 and 0.5.

Bernoulli Monitoring: Operating Characteristic Curves
alpha=beta=0.2
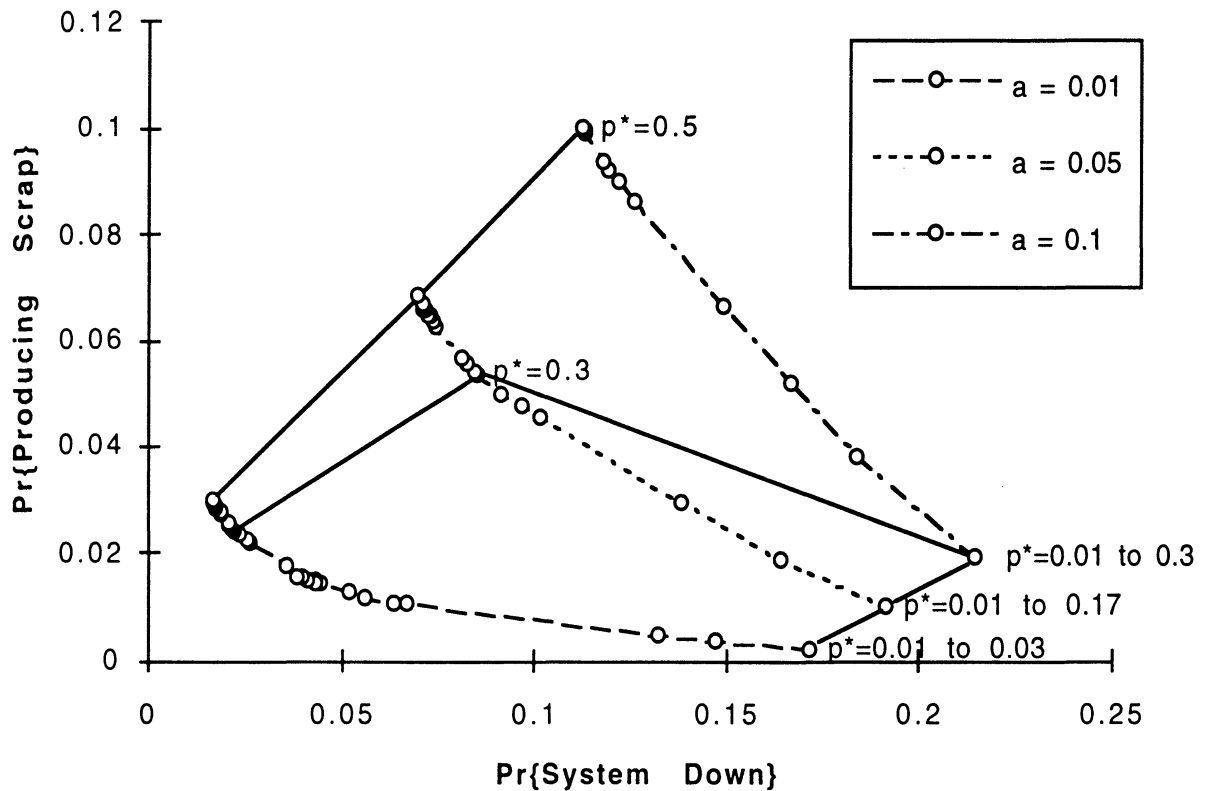
Figure 7.4b: Operating Characteristic Curves of Figure 7.4a but with $\alpha = \beta$ decreased from 0.3 to 0.2. Note that increasing the failure rate tends to collapse ranges of smaller p^* into one operating point, for example $p^* \in (0.01, 0.3)$ produces a wide range of operating points when $a = 0.01$, but produces only *one* operating point when $a = 0.1$. Comparing this figure with Figures 7.4a and 7.4c shows this collapse is more pronounced with smaller α and β.

27

Bernoulli Monitoring: Operating Characteristic Curves
alpha=beta=0.1
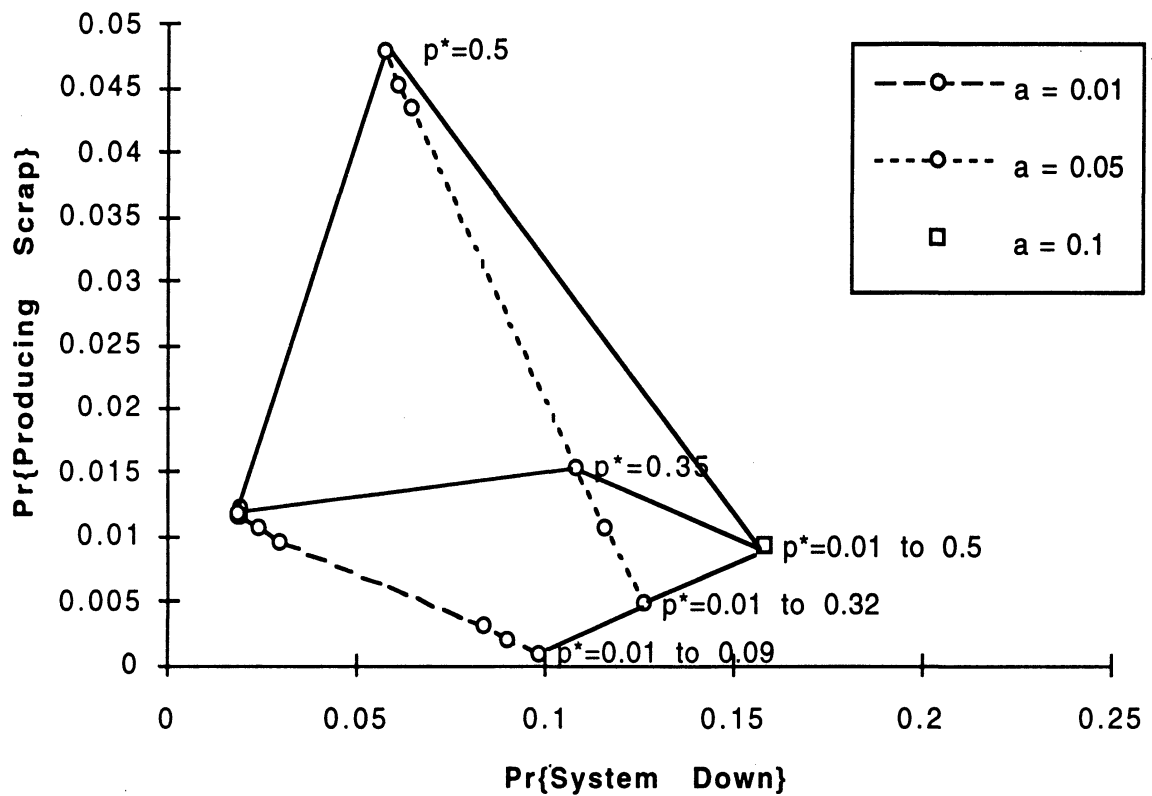
Figure 7.4c: Operating Characteristic Curves of Figure 7.4a with $\alpha = \beta$ reduced from 0.3 to 0.1. Note the extreme collapse of operating points to just one for all $p^* \in (0.01, 0.5)$ associated with a high failure rate $(a = 0.1)$ and informative sensors.

Bernoulli Monitoring: Operating Characteristic Curves
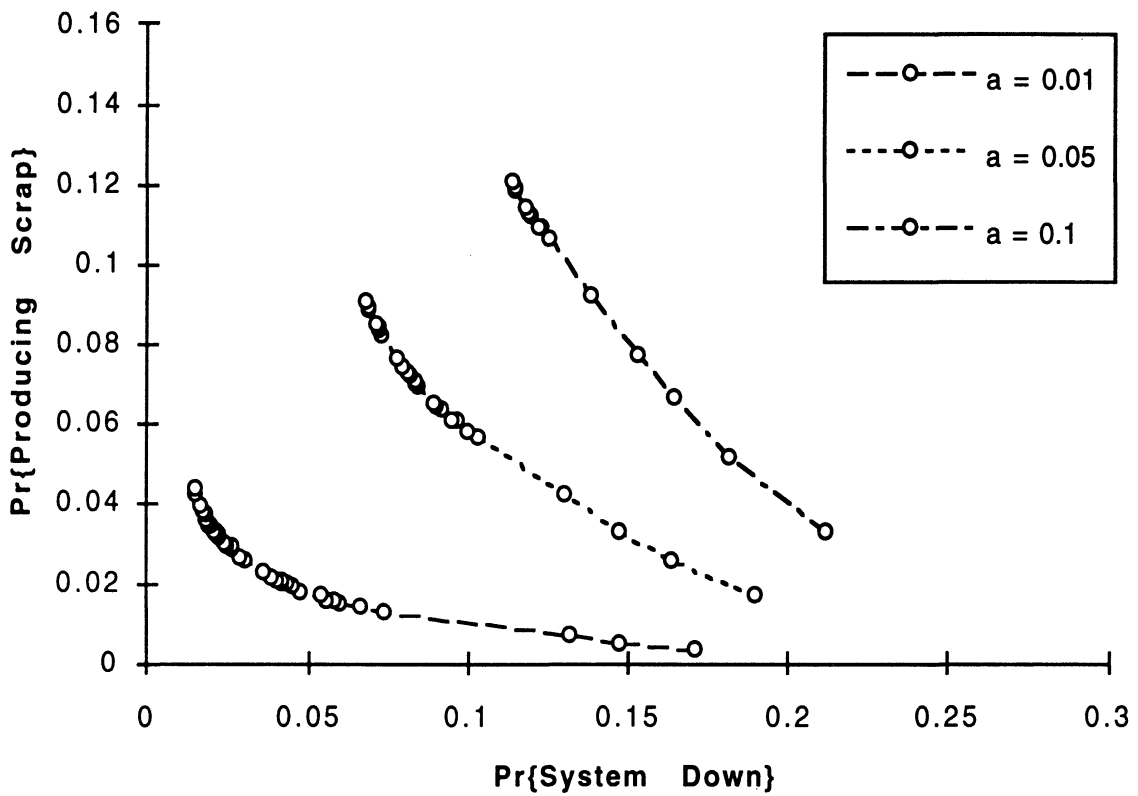**Asymmetric Sensor   alpha=0.3, beta=0.2**

Figure 7.5: Operating Characteristic Curves of Figure 5.4A with an asymmetric sensor: $\alpha = 0.3$, $\beta = 0.2$. Decreasing β from 0.3 (as in Figure 7.4a) to 0.2 (above) improves both performance measures.

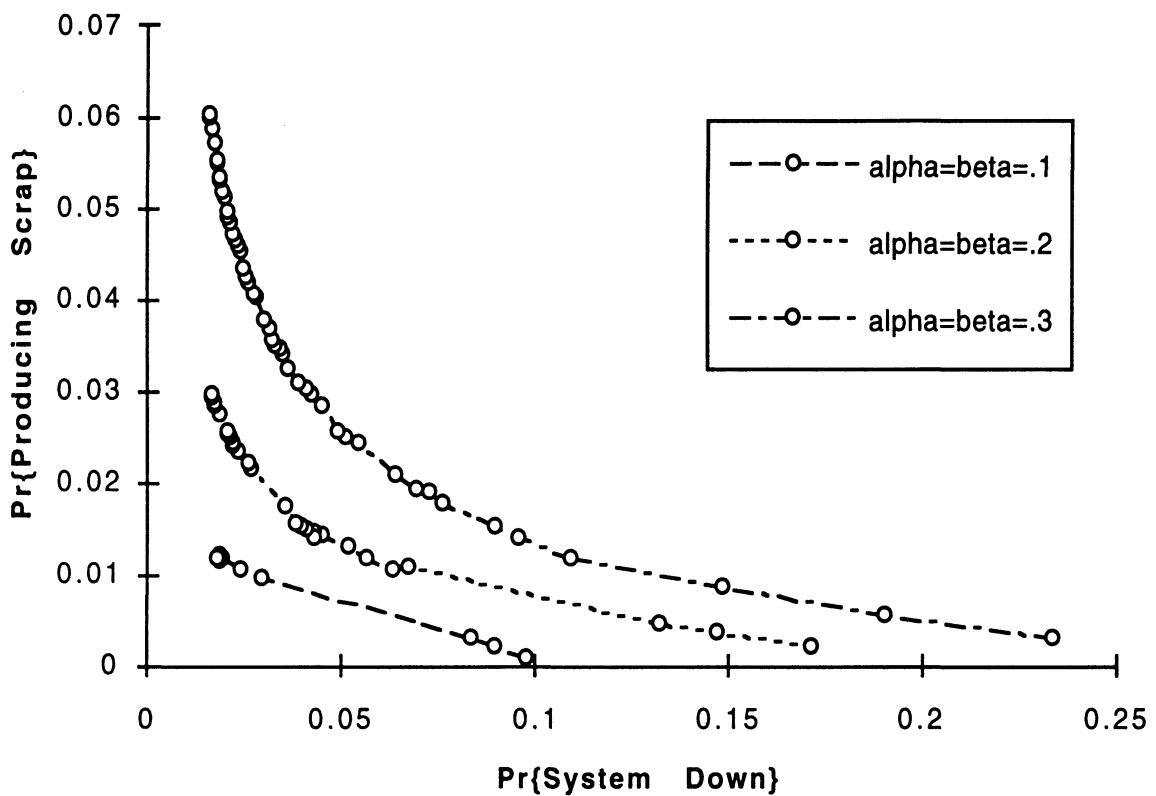**Bernoulli Monitoring: Operating Characteristic Curves**
a= 0.1

Legend:
- alpha=beta=.1
- alpha=beta=.2
- alpha=beta=.3

X-axis: Pr{System Down}
Y-axis: Pr{Producing Scrap}

Figure 7.6: Decreasing α and β of a symetric sensor from 0.3 to 0.1 dramatically improves the Operating Characteristic for scrap production versus system down time.

30

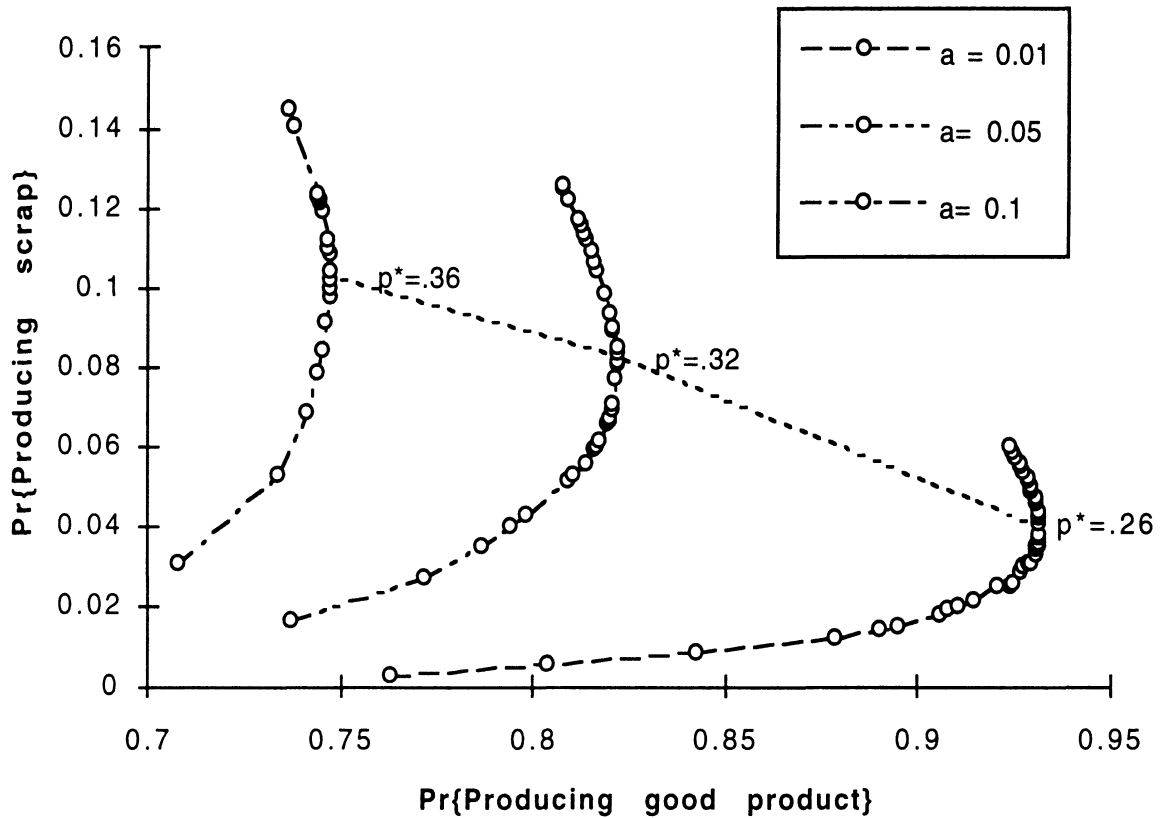**Bernoulli Monitoring: Operating Characteristic Curves**
alpha=beta=0.3

Pr{Producing scrap}

Pr{Producing good product}

- —O— — a = 0.01
- —·—O·—·— a= 0.05
- —·O·— a= 0.1

p*=.36

p*=.32

p*=.26

Figure 7.7: Operating Characteristic Curve for scrap production versus good production. "Better" is towards the point (1,0): no scrapping and always producing good product (no down time). Note the non-optimal operating points above the dotted line: when $a = 0.01$, for example, for each p^* above 0.26 there exists a p^* below 0.26 with the same throughput of good product and a lower scrap rate. Similar "optimality threshold boundaries" for $a = 0.05$ and $a = 0.1$ are near 0.32 and 0.36, respectively.

Normal Monitoring: Probability Density over z
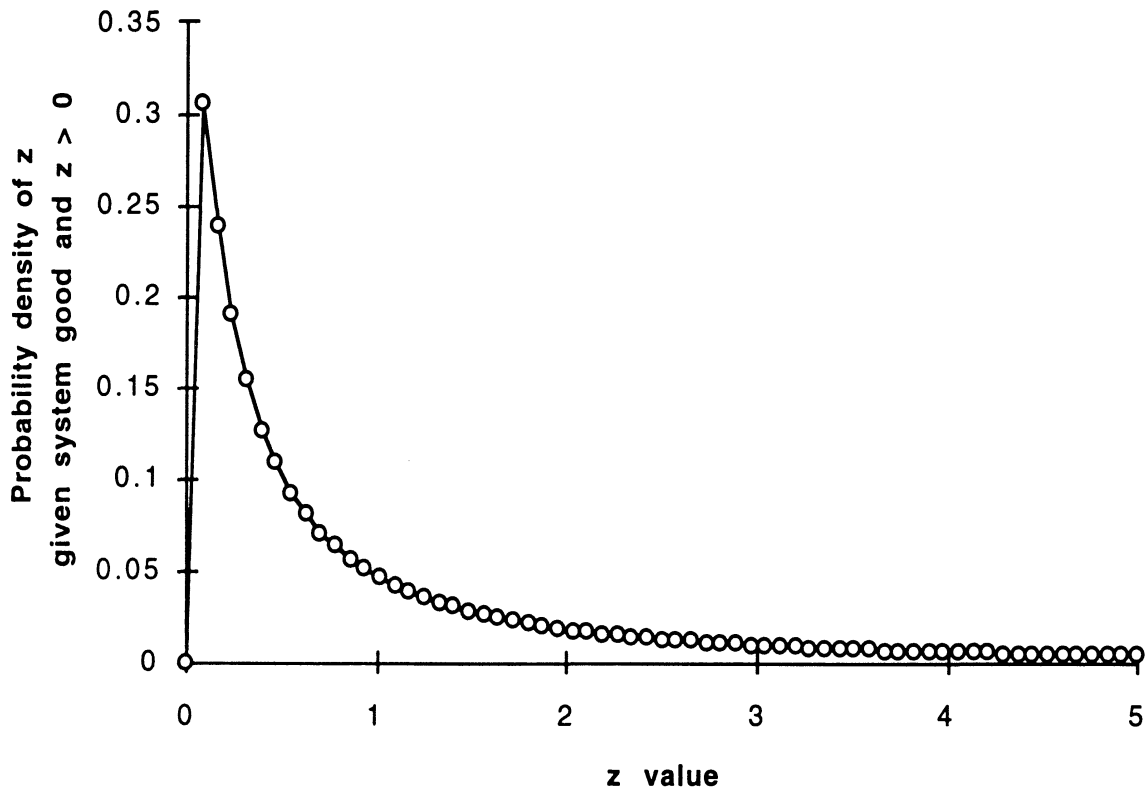**a=0.05,   mu=.5,   p*=0.2**

Figure 8.1: Probability density function $\pi_0 \hat{f}_g(z)$ over states in $\{z : 0 < z < z^*$ and in condition $G\}$ given an alarm threshold of $p* = 0.2$ (or $z^* = 5$). Observations X_n are normally distributed random variables with a variance of 1 and a mean μ that shifts from zero to 0.5 when the system fails. Failure times are geometrically distributed with rate $a = 0.05$. It can be shown that $\lim_{z \to 0} \hat{f}_g(z) = 0$.

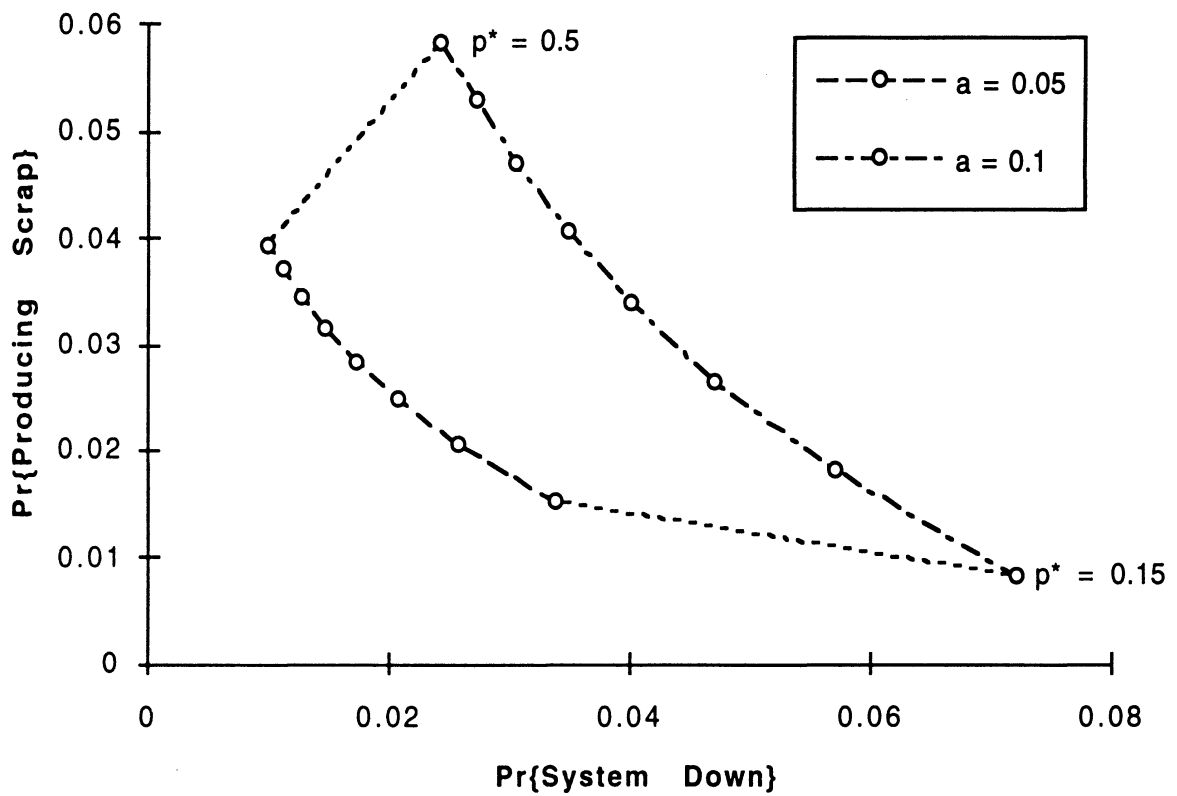**Normal Monitoring: Operating Characteristic Curves**
mu=1.5

Figure 8.2: Operating Characteristic Curves generated by fixing $\mu = 1.5$ and varying p^* from 0.15 to 0.5 in steps of 0.05. Points associated with the same value of p^* are connected by a dotted line for $p^* = 0.15$ and 0.5.

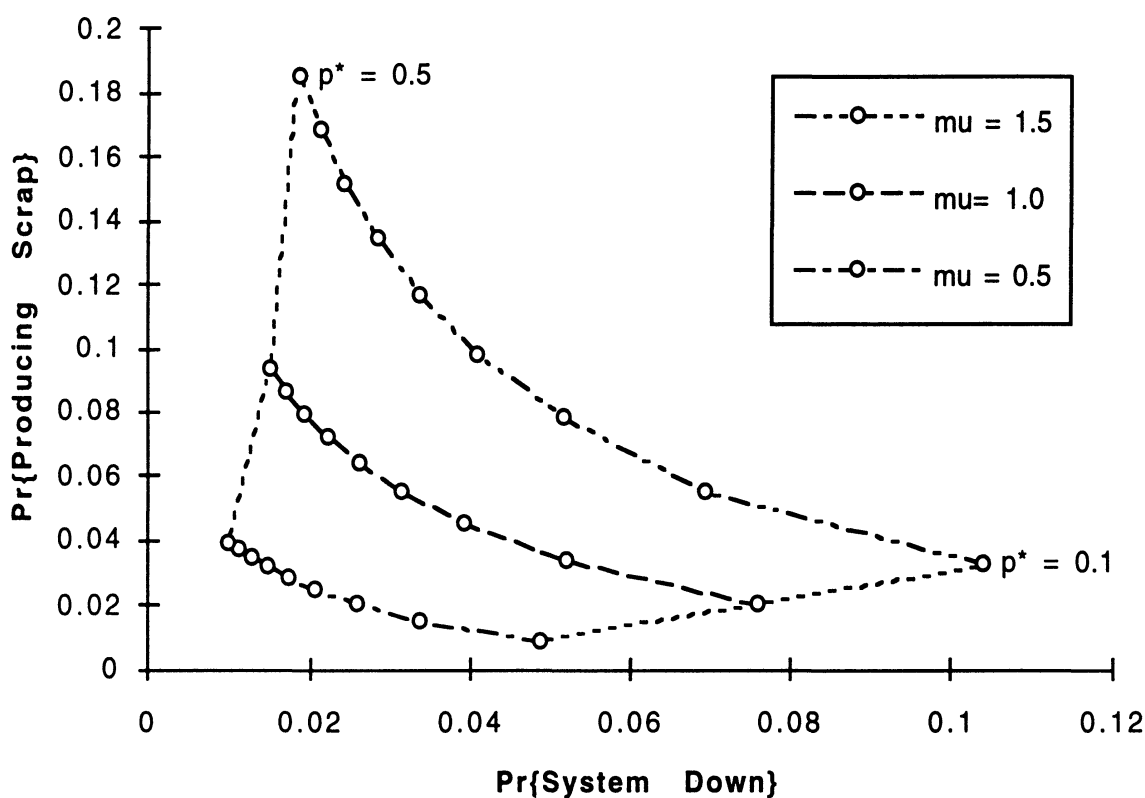**Normal Monitoring: Operating Characteristic Curves**
a = 0.05

Figure 8.3: Operating Characteristic Curves generated by fixing $a = 0.05$ and varying p^* from 0.1 to 0.5 in steps of 0.05. There are three curves: one for each mean observation value $\mu \in \{1.5, 1.0, 0.5\}$. Points associated with the same value of p^* are connected by a dotted line for $p^* = 0.1$ and 0.5. A higher μ implies a more discrimating sensor which improves the Operating Characteristic.
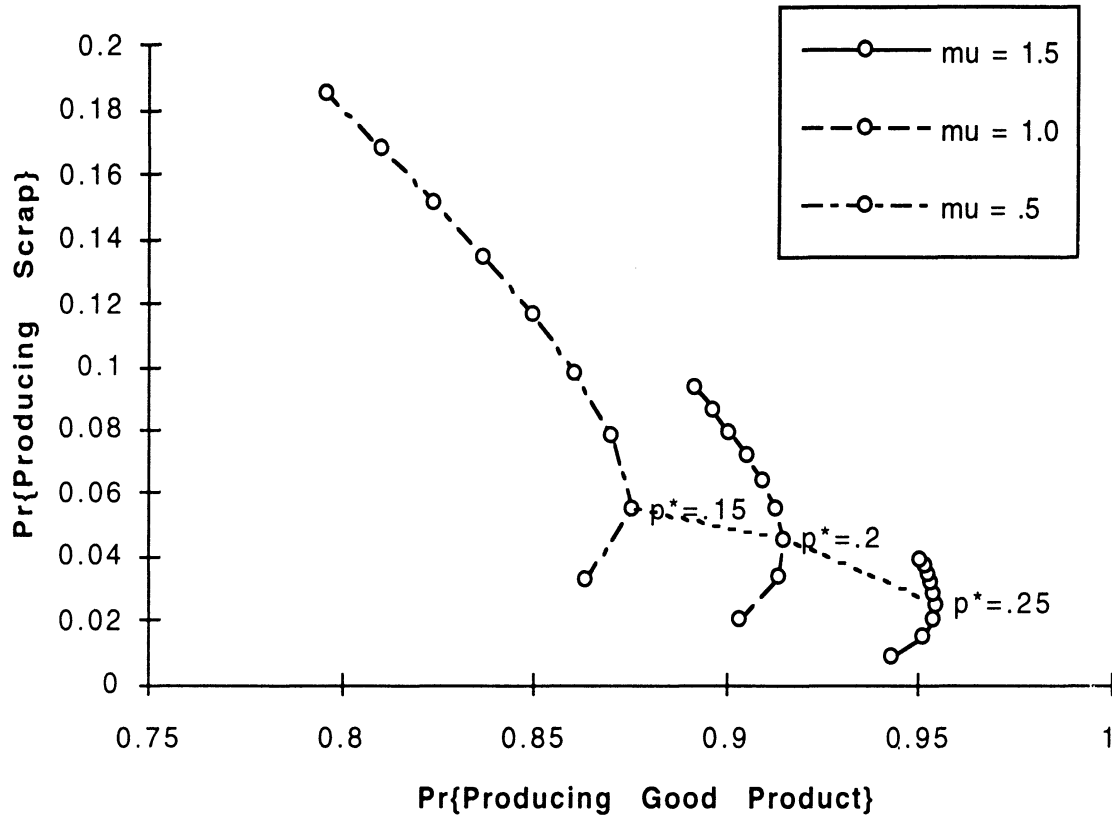
Figure 8.4: Operating Characteristic Curve under Normal monitoring for scrap production versus good production with fixed $a = 0.05$. " Better" is towards the point $(1,0)$: no scrapping and always producing good product (no down time). Note the non-optimal operating points above the dotted line: when $\mu = 1$, for example, for each p^* above 0.2 there exits a p^* below 0.2 with the same throughput of good product *and* a lower scrap rate. Similar "optimality threshold boundaries" for $\mu = 0.5$ and 1.5 are near $p^* = 0.15$ and 0.25, respectively.